JOURNAL OF AIRCRAFT
Vol. 46, No. 4, July–August 2009

Lagwise Loads Analysis of a Rotor Blade with an Embedded Chordwise Absorber

Dong Han* and Edward C. Smith†
Pennsylvania State University, University Park, Pennsylvania 16802

DOI: 10.2514/1.40569

An aeroelastic simulation of a stiff in-plane hingeless rotor in forward flight is conducted to evaluate the feasibility of reducing lagwise root loads via an embedded absorber within the blade. A finite element analysis based on a moderate deflection beam model is employed to capture the flap, lag, and torsion deflections of the rotor blade. The mass-spring-damper absorber system is simulated as a one-degree-of-freedom rigid body with chordwise motion. By using the Hamilton principle, system equations of motion are derived based on the generalized force formulation. Dynamic responses are calculated to investigate the potential of the absorber for in-plane loads reduction. Parametric studies are conducted to explore the influence of the absorber on the dynamic characteristics of the rotor blade. From the aeroelastic analysis of the blade-absorber system, results indicate that placing an embedded absorber in the blade chordwise direction can decrease the 1 and 2/rev lagwise root bending moments by about 50 and 90%, respectively, under large load states. The effects of absorber frequency, absorber damping, chordwise position of the absorber, rotor thrust, forward speed, and trim condition are also studied.

Nomenclature

A	=	blade cross-sectional area
C	=	damping matrix
C_T	=	thrust coefficient
C_{l_α}	=	section lift-curve slope
c	=	chord length
d_{fl}	=	distance from flap hinge to lag hinge
d_{lp}	=	distance from lag hinge to pitch hinge
d_{of}	=	distance from hub center to flap hinge
E	=	elastic modulus
$\mathbf{F}$	=	force vector
f	=	frequency
G	=	shear modulus
K	=	stiffness matrix
l	=	blade length
M	=	mass matrix/moment
m	=	mass
n	=	number of generalized degrees
Q	=	generalized force
q	=	generalized coordinate
$\mathbf{R}$	=	position vector
R	=	rotor radius
t	=	time
U	=	strain energy
u	=	axial elastic displacement
v	=	lagwise elastic displacement
W	=	work done by externally applied forces
w	=	flapwise elastic displacement
x	=	axial coordinate
y_a	=	absorber displacement
y_{a0}	=	initial absorber displacement
y, z	=	section coordinates in undeformed coordinate system
β	=	flap angle
β_{1c}	=	longitudinal tip-path-plane tilt angle
β_{1s}	=	lateral tip-path-plane tilt angle
γ	=	shear strain
δ	=	variation symbol
ε_{xx}	=	axial strain
ζ	=	damping ratio
η, ς	=	section coordinates in deformed coordinate system
θ_p	=	$\theta_0 + \theta_{1c}\cos\psi + \theta_{1s}\sin\psi$
θ_0	=	collective pitch angle
θ_1	=	$\theta_t + \phi$
θ_{1c}	=	lateral cyclic pitch angle
θ_{1s}	=	longitudinal cyclic pitch angle
θ_t	=	pretwist
λ	=	inflow
μ	=	advance ratio
ν_ζ	=	lag frequency
ρ	=	blade density
ϕ	=	torsional deformation
ψ	=	azimuth/warping function
Ω	=	rotor speed

Subscripts

a	=	contribution from absorber
i, j	=	trix or vector index
$()_\eta$	=	$\frac{\partial()}{\partial\eta}$
$()_\varsigma$	=	$\frac{\partial()}{\partial\varsigma}$

Superscripts

A	=	contribution from aerodynamics
a	=	contribution from absorber
E	=	contribution from elastic potential energy
T	=	contribution from kinetic energy
$'$	=	$\frac{\partial}{\partial x}$
$\cdot$	=	$\frac{\partial}{\partial t}$

Presented as Paper 2182 at the 49th AIAA/ASME/ASCE/AHS/ASC Structures, Structural Dynamics, and Materials Conference 16th AIAA/ASME/AHS Adaptive Structures Conference 10t, Schaumburg, IL, 7–10 April 2008; received 24 August 2008; revision received 22 December 2008; accepted for publication 24 January 2009.

*Research Associate, Aerospace Engineering, 229 Hammond Building. Member AIAA.

†Professor, Aerospace Engineering, 231D Hammond Building. Member AIAA.

I. Introduction

FOR articulated or soft in-plane hingeless rotors, ground or air resonance will occur under certain conditions. The cause of these instabilities is related to rotor–body inertial coupling and the

weak lag mode damping provided by the aerodynamics. Strong mechanical dampers must be added to the rotor system at the blade root and to the fuselage landing gear supports to control these instabilities. These instabilities do not occur in stiff in-plane rotors (i.e., lag frequency above 1/rev); hence, lag dampers are unnecessary. In addition, stiff in-plane hingeless rotors can be generally lighter weight and are attractive for large rotor designs. However, stiff in-plane rotors exhibit loads in the lagwise direction, which are much higher than in articulated or soft in-plane rotors. These high loads can result in undesirable weight penalties and higher fuselage vibration levels.

Consider a rigid rotating blade with lag hinge spring and without hinge offset. The 1/rev motion due to the aerodynamic and Coriolis forces is proportional to $1/(1-v_\zeta^2)$ [1] if other parameters are fixed. Because the spring stiffness is proportional to v_ζ^2, the 1/rev lagwise root bending moment is proportional to $v_\zeta^2/(1-v_\zeta^2)$. Similarly, the 2/rev lagwise root bending moment is proportional to $v_\zeta^2/(4-v_\zeta^2)$. The curve $v_\zeta^2/|1-v_\zeta^2|$ versus v_ζ could be used to illustrate the typical 1/rev lagwise load, shown in Fig. 1. The curve $v_\zeta^2/|4-v_\zeta^2|$ versus v_ζ could be used to illustrate the typical 2/rev lagwise load, shown in Fig. 2. These figures illustrate that the 1/rev load of typical stiff in-plane blades in the lagwise direction ($v_\zeta = 1.4$) is about 2 times that of typical soft in-plane blades ($v_\zeta = 0.7$) and the ratio is about 7 for the 2/rev load. If the 1 and 2/rev loads of the stiff in-plane blade need to be decreased to the level of the soft in-plane blade, about 50% for the 1/rev load and 85% for the 2/rev load are to be reduced.

Larger rotor loads mean that the blade weight has to be increased to enhance the structural integrity and fatigue life, the control system must be designed to withstand higher loads, the damage tolerance can decrease, and so on. It is a challenging task to decrease the lagwise loads in rotor blade design, especially with the emergence of lightweight stable stiff in-plane rotors.

Zapfe and Lesieutre put forward the concept of distributed inertial dampers using chordwise absorbers to provide damping to the beam structure [2]. Their computational studies demonstrated the effectiveness of using a simply supported beam under tensile load. Hébert and Lesieutre adopted highly distributed tuned vibration absorbers to provide lag damping to helicopter blades [3]. Their computational studies pointed out that the method could provide enough damping comparable to or better than the methods already in use or proposed with a weight penalty equal to only 3%. Kang et al. carried out a comprehensive analysis of the damping characteristics of a rotor blade with an embedded chordwise absorber [4–6]. Petrie et al. used an embedded fluid-elastomer absorber to enhance blade lag damping and conducted the fluid-elastomer design and the lag damping test of a blade with a fluid-elastomer absorber [7,8].

Previous research studies concentrated on how much damping the embedded chordwise absorber could provide to the soft in-plane or articulated rotor blades. Because loads of stiff in-plane rotors in the lagwise direction can be much higher than soft in-plane rotors, the present paper will focus on the achieved lagwise loads using embedded chordwise absorbers and concentrate on how much loads can be reduced using 10% blade mass, as shown in Fig. 3. As a first step, a nonrotating cantilever blade with a chordwise absorber is analyzed to investigate the dynamics of the blade-absorber system. Then the feasibility of this concept of reducing the 1 and 2/rev lagwise loads of stiff in-plane blades to the level of soft in-plane blades with about 10% blade mass is explored. Finally, a comprehensive investigation is carried out to explore the effects of parameters such as tuning frequency, damping, mass, chordwise position, and flight state.

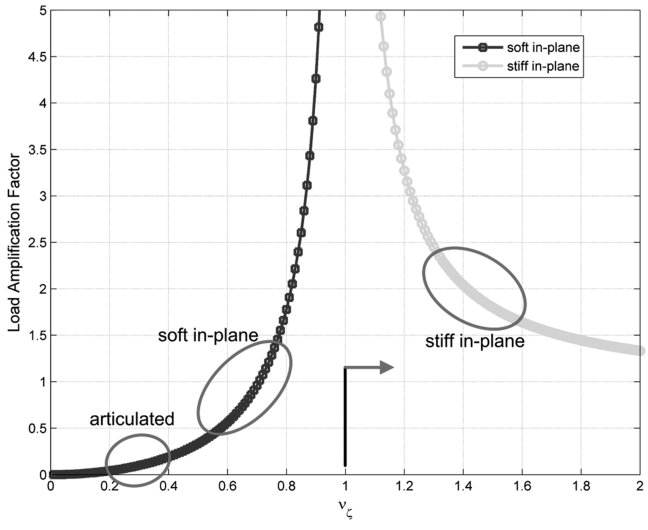

Fig. 1 Typical 1/rev lagwise load.

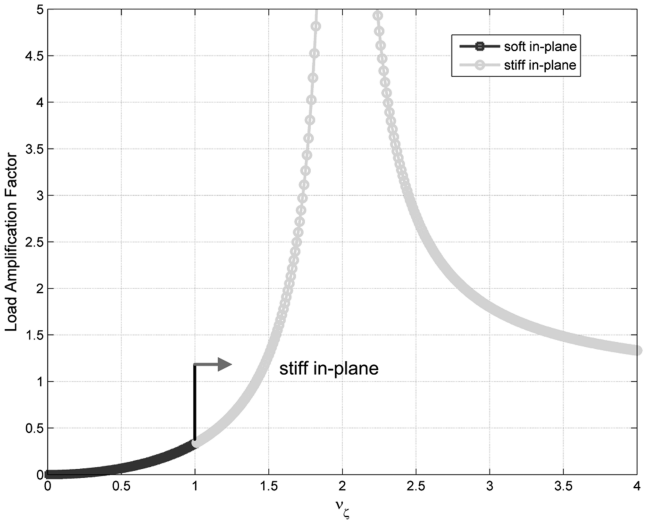

Fig. 2 Typical 2/rev lagwise load.

II. Model

A. Moderate Deflection Beam Model

To describe the geometrical nonlinearity of advanced helicopter blades, such as hingeless and bearingless rotor blades, Hodges and Dowell put forward the moderate deflection beam model [9]. The modified moderate deflection beam model is adopted in this paper [10]. The axial strain and shear strains of arbitrary point (x, η, ς) on the blade are

$$\varepsilon_{xx} = u' + (v'^2/2) + (w'^2/2) + (\psi\phi')' + \tfrac{1}{2}(\eta^2+\varsigma^2)\phi'^2 - y[v''(1-\phi^2/2) + w''\phi] - z[-v''\phi + w''(1-\phi^2/2)] \quad (1)$$

$$\gamma_{x\eta} = (\psi_\eta - \varsigma)(\phi' + v''w') \quad (2)$$

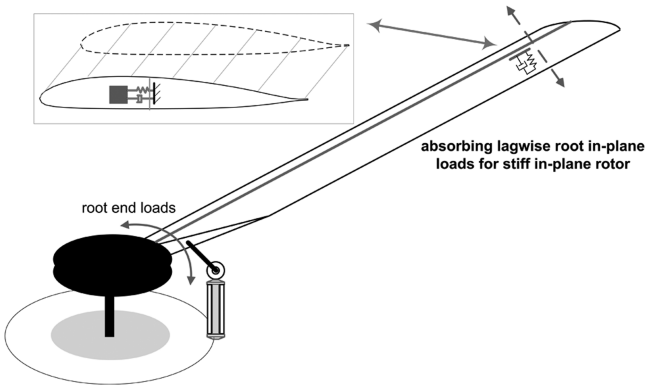

Fig. 3 Configuration of stiff in-plane rotor blade with an embedded absorber.

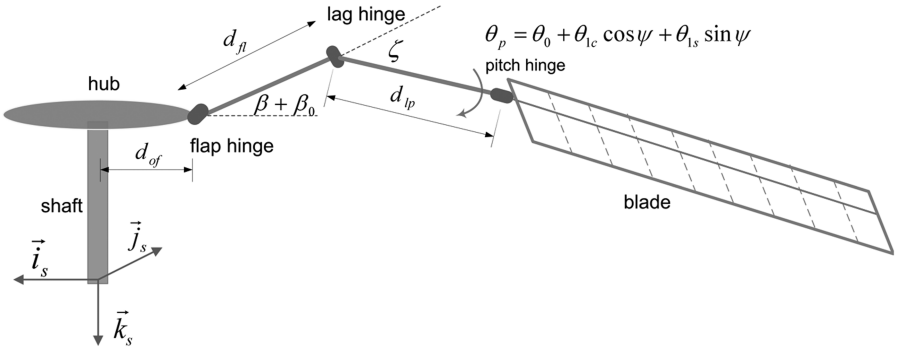

Fig. 4 Blade configuration.

$$\gamma_{x\varsigma} = (\psi_\varsigma + \eta)(\phi' + v''w') \tag{3}$$

and the variation of the elastic potential energy is

$$\delta U = \sum_{i=1}^{n} Q_i^E \delta q_i = \int_l \iint_A (E\varepsilon_{xx}\delta\varepsilon_{xx} + G\gamma_{x\eta}\delta\gamma_{x\eta} + G\gamma_{x\varsigma}\delta\gamma_{x\varsigma})\,\mathrm{d}A\,\mathrm{d}l \tag{4}$$

B. Kinetic Energy

Helicopter rotor blades not only have elastic deflections, but they also have rigid motions. Adoption of both the moderate deflection beam model and finite rotations would make the calculation of kinetic energy much more complicated. To better describe the nonlinear coupling characteristics between elastic deflections and rigid motions for rotor blades, the computational method for kinetic energy based on generalized force formulation, derived by Zheng et al. [11], is adopted. The rigid motions of the flap, lag, and pitch hinges are introduced as generalized coordinates, as shown in Fig. 4. The hinge sequences can be changed according to actual rotors. When the three rigid rotational generalized coordinates are adopted, the modeling methodology can suit other types of helicopter rotors. For example, when calculating the transient aeroelastic response of teetering rotors, the degrees of the lag and pitch hinges need to be constrained, and the method used by Keller [12] is adopted to coordinate the flap hinge degree. When calculating the kinetic energy, warping effect is usually not taken into account. The position vector of an arbitrary point on the blade in a rotor shaft coordinate frame is

$$\begin{Bmatrix} R_{sx} \\ R_{sy} \\ R_{sz} \end{Bmatrix}^T = \begin{Bmatrix} d_{of} \\ 0 \\ 0 \end{Bmatrix}^T [T_{rs}] + \begin{Bmatrix} d_{\mathrm{fl}} \\ 0 \\ 0 \end{Bmatrix}^T [T_{fr}][T_{rs}] + \begin{Bmatrix} d_{\mathrm{lp}} \\ 0 \\ 0 \end{Bmatrix}^T [T_{lf}][T_{fr}][T_{rs}] + \begin{Bmatrix} x+u \\ v \\ w \end{Bmatrix}^T [T_{pl}][T_{lf}][T_{fr}][T_{rs}] + \begin{Bmatrix} 0 \\ \eta \\ \varsigma \end{Bmatrix}^T [T][T_{pl}][T_{lf}][T_{fr}][T_{rs}] \tag{5}$$

where these transformation matrices are defined in the Appendix. Thus, the variation of the kinetic energy of a blade [11] is

$$\delta T = \sum_{i=1}^{n} Q_i^T \delta q_i = \sum_{i=1}^{n} \int_l \iint_A -\rho\ddot{\mathbf{R}} \cdot \frac{\partial \mathbf{R}}{\partial q_i}\,\mathrm{d}A\,\mathrm{d}l\delta q_i \tag{6}$$

and its ith generalized force introduced by the kinetic energy is

$$Q_i^T = \int_l \iint_A -\rho\ddot{\mathbf{R}} \cdot \frac{\partial \mathbf{R}}{\partial q_i}\,\mathrm{d}A\,\mathrm{d}l \tag{7}$$

According to the definition of tangent mass, damping, and stiffness matrices introduced by kinetic energy, the expressions of these matrices are

$$M_{ij}^T = \frac{\partial Q_i^T}{\partial \ddot{q}_j} = -\int_l \iint_A \rho \frac{\partial \mathbf{R}}{\partial q_j} \cdot \frac{\partial \mathbf{R}}{\partial q_i}\,\mathrm{d}A\,\mathrm{d}l \tag{8}$$

$$C_{ij}^T = \frac{\partial Q_i^T}{\partial \dot{q}_j} = -\int_l \iint_A 2\rho \frac{\partial \dot{\mathbf{R}}}{\partial q_j} \cdot \frac{\partial \mathbf{R}}{\partial q_i}\,\mathrm{d}A\,\mathrm{d}l \tag{9}$$

$$K_{ij}^T = \frac{\partial Q_i^T}{\partial q_j} = -\int_l \iint_A \rho\left(\frac{\partial \ddot{\mathbf{R}}}{\partial q_j} \cdot \frac{\partial \mathbf{R}}{\partial q_i} + \ddot{\mathbf{R}} \cdot \frac{\partial^2 \mathbf{R}}{\partial q_i \partial q_j}\right)\mathrm{d}A\,\mathrm{d}l \tag{10}$$

From the expressions of tangent mass, damping, and stiffness matrices and the generalized force vector, it can be seen that, if these matrices are calculated, the position vector of an arbitrary point on the blade shown in Eq. (5) and its derivative with respect to time and partial derivatives with respect to generalized coordinates need to be given out.

C. Aerodynamics

In the present paper, a nonlinear quasi-steady aerodynamic model is adopted, and the lift, drag, and moment coefficients of the airfoil are calculated by a two-dimensional table-look-up method according to the angle of attack and the oncoming air flow (Mach number). The direction of blade section velocity is shown in Fig. 5. The velocity of an arbitrary point on the pitch axis with respect to the local airflow is

$$\begin{Bmatrix} U_R \\ U_T \\ U_P \end{Bmatrix}^T = \begin{Bmatrix} \dot{R}_{sx} \\ \dot{R}_{sy} \\ \dot{R}_{sz} \end{Bmatrix}^T \{[T][T_{pl}][T_{lf}][T_{fr}][T_{rs}]\}^T - \begin{Bmatrix} -\mu_1 \\ -\mu_2 \\ \lambda - \mu_3 \end{Bmatrix}^T [T_{tps}]\{[T][T_{pl}][T_{lf}][T_{fr}][T_{rs}]\}^T \tag{11}$$

where μ_1, μ_2, and μ_3 are the components of the air velocity in the rotor tip plane. Using a nonlinear quasi-steady aerodynamic model, the forces introduced by the aerodynamics can be calculated using

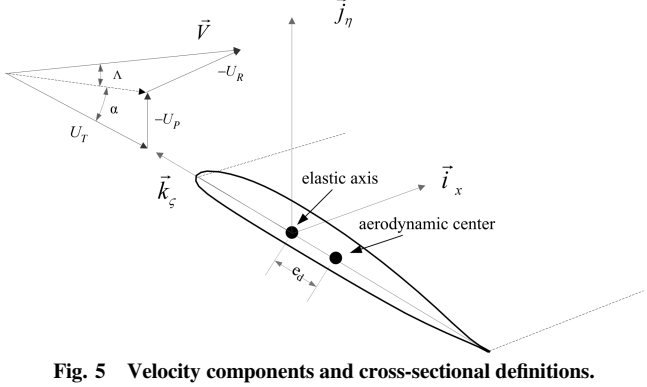

Fig. 5 Velocity components and cross-sectional definitions.

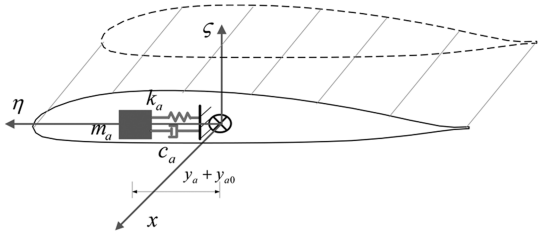

Fig. 6 Coordinate system of rotor blade with embedded chordwise absorber.

the velocity expression, Eq. (11). The variation of the work done by the aerodynamics is

$$\delta W^A = \sum_{i=1}^{n} Q_i^A \delta q_i = \int_l (\mathbf{F}_A \cdot \delta \mathbf{R}_s + \mathbf{M}_A \cdot \delta \mathbf{a}_s)\, \mathrm{d}l \tag{12}$$

The generalized force introduced by the aerodynamics is

$$Q_i^A = \int_l \left(\mathbf{F}_A \cdot \frac{\partial \mathbf{R}_s}{\partial q_i} + \mathbf{M}_A \cdot \frac{\partial \mathbf{a}_s}{\partial q_i} \right) \mathrm{d}l \tag{13}$$

It should be noted that the force vector $\mathbf{F}_A$, moment vector $\mathbf{M}_A$, position vector $\mathbf{R}_s$, and angle vector $\mathbf{a}_s$ are defined in the rotor shaft coordinate system, which is treated as an inertial coordinate system. Thus, after the aerodynamic forces and moments in the deformed coordinate system are calculated, these vectors must be transformed to the rotor shaft coordinate system. The Pitt–Peters dynamic inflow model is used to capture the induced velocity [13].

D. Embedded Chordwise Absorber

The absorber is treated as a one-degree-of-freedom rigid body with chordwise motion, as shown in Fig. 6. The device is mechanically constrained to move only in the blade chordwise direction. The relative displacement of the absorber to the blade is denoted as $y_{a_0} + y_a$. The position vector of the absorber can be expressed as

$$\begin{aligned}
\begin{Bmatrix} R_{ax} \\ R_{ay} \\ R_{az} \end{Bmatrix}^T &= \begin{Bmatrix} d_{of} \\ 0 \\ 0 \end{Bmatrix}^T [T_{rs}] + \begin{Bmatrix} d_{\mathrm{fl}} \\ 0 \\ 0 \end{Bmatrix}^T [T_{fr}][T_{rs}] \\
&+ \begin{Bmatrix} d_{\mathrm{lp}} \\ 0 \\ 0 \end{Bmatrix}^T [T_{lf}][T_{fr}][T_{rs}] + \begin{Bmatrix} x+u \\ v \\ w \end{Bmatrix}^T [T_{pl}][T_{lf}][T_{fr}][T_{rs}] \\
&+ \begin{Bmatrix} 0 \\ y_a + y_{a_0} \\ 0 \end{Bmatrix}^T [T][T_{pl}][T_{lf}][T_{fr}][T_{rs}]
\end{aligned} \tag{14}$$

Inserting the expression of the position vector of the absorber in Eqs. (7–10), the generalized force, tangent mass, damping, and stiffness matrices can be attained. The elastic potential energy is $\frac{1}{2} k_a y_a^2$, and the work done by the viscous force is $\frac{1}{2} c_a \dot{y}_a^2$. The absorber thus contributes to the generalized force, tangent stiffness, and damping matrices.

E. Equations of Motion

According to the Hamilton principle, the implicit nonlinear dynamic equations based on generalized force formation include four parts: elastic potential energy, kinetic energy, work done by the aerodynamics, and energy stored by the absorber. The equations of motion based on the generalized force formulation are

$$\begin{aligned}
&Q_i^T(\mathbf{q}, \dot{\mathbf{q}}, \ddot{\mathbf{q}}, t) + Q_i^E(\mathbf{q}) + Q_i^A(\mathbf{q}, \dot{\mathbf{q}}, t) + Q_i^a(\mathbf{q}, \dot{\mathbf{q}}, \ddot{\mathbf{q}}, t) = 0 \\
&\qquad (i = 1, \ldots, n)
\end{aligned} \tag{15}$$

After assembling the mass, damping, and stiffness matrices introduced by the four components, the corresponding matrices of the system can be determined. An implicit Newmark integration method is adopted to calculate the dynamic responses [14].

F. Wind-Tunnel Trim Analysis

When the steady-state response is calculated, the corresponding pitch controls to the rotor need to be provided. In the present paper, the wind-tunnel trim method [15] is adopted to trim the rotor. The control input vector is $\mathbf{x} = \{\, \theta_0 \quad \theta_{1c} \quad \theta_{1s} \,\}^T$, and the output or target vector is $\mathbf{y} = \{\, C_T \quad \beta_{1c} \quad \beta_{1s} \,\}^T$. According to the Newton–Raphson method, the recursive expression to calculate the pitch controls in the nth step is

$$\mathbf{x_n} = \mathbf{x_{n-1}} + \mathbf{J^{-1}}(\mathbf{y} - \mathbf{y_{n-1}}) \tag{16}$$

where the Jacobian matrix is

$$[J] = \begin{bmatrix} \frac{\partial C_T}{\partial \theta_0} & \frac{\partial C_T}{\partial \theta_{1c}} & \frac{\partial C_T}{\partial \theta_{1s}} \\ \frac{\partial \beta_{1c}}{\partial \theta_0} & \frac{\partial \beta_{1c}}{\partial \theta_{1c}} & \frac{\partial \beta_{1c}}{\partial \theta_{1s}} \\ \frac{\partial \beta_{1s}}{\partial \theta_0} & \frac{\partial \beta_{1s}}{\partial \theta_{1c}} & \frac{\partial \beta_{1s}}{\partial \theta_{1s}} \end{bmatrix} \tag{17}$$

Because the precision of the Jacobian matrix only influences the number of iterations, simple expressions of the partial derivatives are adopted to give approximations. For example, the analytical expression for the thrust coefficient [16] is

$$\begin{aligned}
C_T = (\sigma C_{l\alpha}/2)[(\theta_0/3)(1 + \tfrac{3}{2}\mu^2) + (\theta_t/4)(1 + \mu^2) \\
+ (\mu/2)\theta_{1s} - (\lambda/2)]
\end{aligned} \tag{18}$$

According to Eq. (18), the partial derivatives associated with the thrust coefficient are

$$\begin{aligned}
\partial C_T/\partial \theta_0 = (\sigma C_{l\alpha}/6)(1 + \tfrac{3}{2}\mu^2), \qquad \partial C_T/\partial \theta_{1c} = 0 \\
\partial C_T/\partial \theta_{1s} = \sigma C_{l\alpha}\mu/4
\end{aligned} \tag{19}$$

The other partial derivatives can also be derived in the same way.

G. Steady Loads Calculation

Trimmed values of pitch controls need to be found before the calculation of the steady rotor response. At first, some prescribed pitch controls are initialized. The wind-tunnel trim method is used to update the pitch controls after every circle integration. Then, the steady response can be attained after several circle iterations. Because the externally applied forces, including the centrifugal force and inertial force, are reacted by the structure, the root bending moments are calculated using the generalized structural forces corresponding to the degrees of freedom. For example, the variation of the elastic potential energy can be expressed as

$$\delta U = \sum F_i \delta q_i (i = 1, \ldots, n)$$

where the generalized degrees are independent. If the structural lagwise root bending moment in the blade coordinate frame is desired, the moment is the generalized nodal force $F_{v'}$ corresponding to the degree v' at the blade root. Because of pitch controls, transformation needs to be conducted to transform the bending moments from the blade coordinate frame to the hub coordinate frame. At last, the 1 and 2/rev lagwise root bending moments from the periodic response of the lagwise root bending moment are extracted.

Fig. 7 Configuration of the nonrotating beam.

Table 1 Parameters of the uniform blade

Parameter	Value	Parameter	Value
Length, m	6.0	Axial stiffness, N	1.0×10^8
Mass, kg	60.0	Flapwise stiffness, Nm^2	1.875×10^5
Flapwise cross-sectional moment of inertia, kg · m	0.05	Lagwise stiffness, Nm^2	1.848×10^6
Lagwise cross-sectional moment of inertia, kg · m	0.2	Torsional stiffness, Nm^2	8.157×10^4

Table 2 First five frequencies of the uniform blade

Mode	Frequency, Hz
1 (F)	2.22
2 (F)	13.2
1 (L)	6.68
2 (L)	41.8
1 (T)	23.8

III. Analysis of Nonrotating Cantilever Blade with Single Absorber

To have a comprehensive understanding of the influences of the absorber system on the dynamic characteristics of the rotor blade, a uniform blade with a mass-spring-damper absorber at the blade tip is adopted to discuss the parameter influences, as shown in Fig. 7. The parameters of the blade are shown in Table 1. Ten to fifteen degree-of-freedom beam elements are adopted to discretize the blade. The natural frequencies are listed in Table 2 (including the first two flap (F) modes, the first two lag (L) modes and the first torsional (T) mode).

Because the natural frequency of the first lag mode is 6.680 Hz, 5 Hz harmonic excitation force $F = 1000\sin(10\pi t)N$ is applied at the blade tip in the lagwise direction to model a stiff in-plane blade excited by the 1/rev lagwise load. A 1% critical structural damping for the first and second lagwise modes is applied to the blade to damp out the transient component of the dynamic response. The time history of the lagwise root bending moment is shown in Fig. 8, in which the steady response is a 5 Hz harmonic response.

An elastomeric absorber is attached to the blade tip, with $m_a = 10$ kg and $\zeta_a = 0.1$. The spring stiffness of the absorber is changed to investigate the influence of the natural frequency on the lagwise root bending moment. The moment ratios with the increase of the natural frequency of the absorber are shown in Fig. 9. The vertical axial corresponds to the ratio of the peak moment for the blade with an absorber to the peak moment for the blade without an absorber in a steady periodic state. From Fig. 9, the following can be concluded:

1) If the natural frequency of the absorber is less than the excitation frequency (5 Hz), the ability of the absorber increases with the increase of the natural frequency of the absorber.

2) When the natural frequency of the absorber is larger than 5 Hz, the ability of the absorber decreases with the increase of the natural frequency.

The tuning frequency of the elastomeric absorber is the excitation frequency, just as it is in the classic Frahm vibration absorber [17].

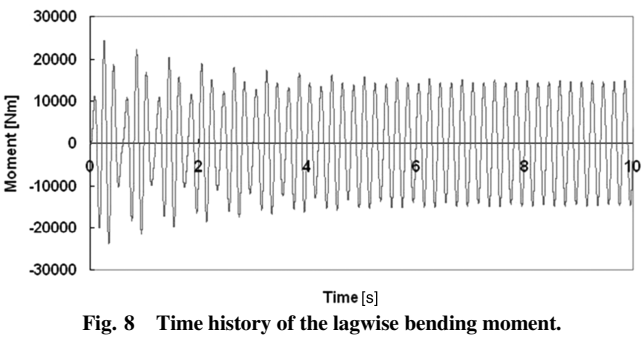

Fig. 8 Time history of the lagwise bending moment.

The natural frequency of the absorber is now set to 5 Hz and the damping ratio to 0.1. The influence of the mass of the absorber on the lagwise root bending moment of the blade is shown in Fig. 10. The vibratory lag moment decreases with an increase in absorber mass. A similar trend is illustrated in Fig. 11, with a decrease in absorber motion amplitude when the absorber mass is increased. Assuming an absorber mass equal to 10% of the blade mass with 10% critical damping, the present analysis predicts that the lagwise root bending moment can be reduced to less than 50% of the baseline value.

To investigate the influence of the damping of the absorber on the lagwise root bending moment and the displacement of the absorber, the absorber mass is then set to 6.0 kg and the natural frequency to 5.0 Hz. The moment and displacement are shown in Figs. 12 and 13, in which the damping ratio varies from 0 to 0.5. These figures illustrate that the lagwise root bending moment increases with the increase in the damping ratio and that the displacement of the absorber decreases. The time history of the lagwise root bending moment with $f_a = 5.0$ Hz, $m_a = 6.0$ kg, and $\zeta_a = 0.1$ is shown in Fig. 14, in which the response in the steady state subjected to the absorber only contains the component of operation frequency and the transient component has been damped out. The time history of the absorber displacement is shown in Fig. 15. The magnitude of the absorber displacement in the chordwise direction is significant and corresponds to 2.8% of the blade length (33.6 cm peak to peak).

The parameters of the absorber are now set to $f_a = 5.0$ Hz, $m_a = 6.0$ kg, and $\zeta_a = 0.1$. The variation of the lagwise moment ratio with respect to the axial installation position of the absorber is shown in Fig. 16, which illustrates that the best place for the absorber is the blade tip. For the convenience of production and maintenance, it is better to install chordwise absorbers at blade tips.

IV. Aeroelastic Analysis of Stiff In-Plane Rotor Blade with an Embedded Absorber

In this section, the aeroelastic analysis of a blade-absorber system in forward flight is presented. A comprehensive parametric analysis is conducted to investigate the loads reduction ability of the 1 and 2/rev absorbers. Potential obstacles to the application of the embedded chordwise absorber to reduce the lagwise loads are discussed.

A. Blade and Absorber Parameters

The baseline blade is a nonuniform stiff in-plane blade, illustrated in Fig. 17. The blade mass density from 70 to 80% and from 90 to 100% of the blade radius is 14 kg/m, and the density at other spanwise locations is 9 kg/m. To keep the same net weight of the two

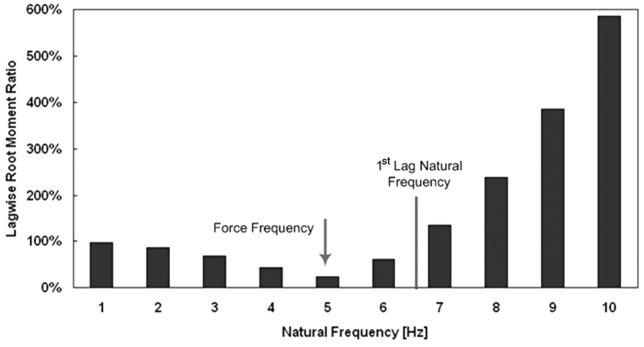

Fig. 9 Influence of the frequency of the absorber on the lagwise moment.

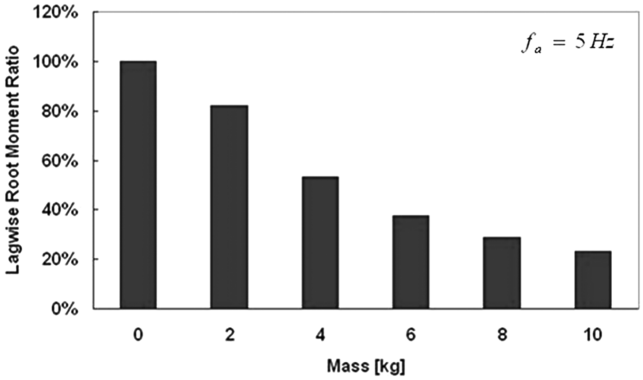

Fig. 10 Influence of the mass of the absorber on the lagwise moment.

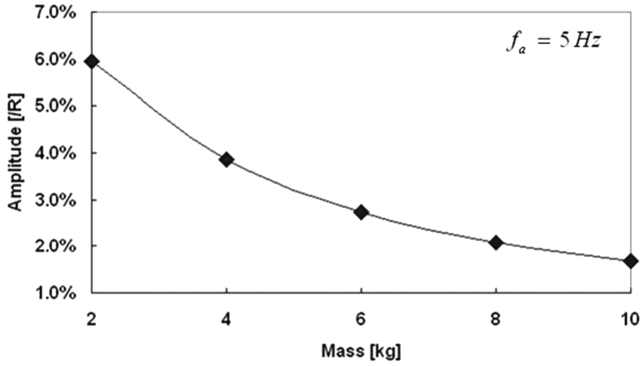

Fig. 11 Influence of the mass of the absorber on the displacement of the absorber.

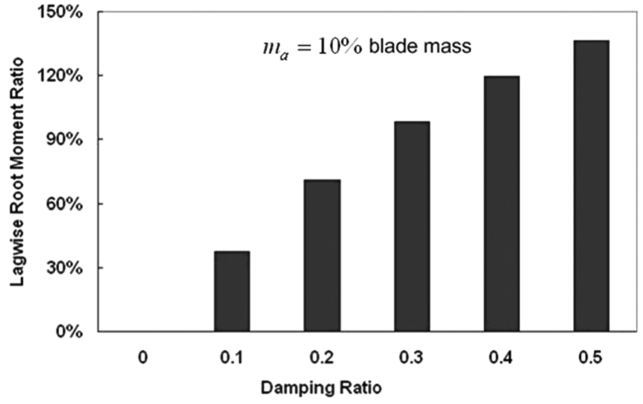

Fig. 12 Influence of the damping of the absorber on the lagwise moment (absorber: 5 Hz).

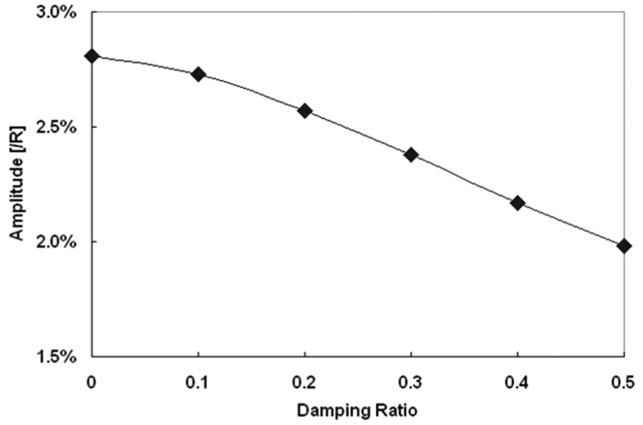

Fig. 13 Influence of the damping of the absorber on the displacement of the absorber.

blade systems, the mass density of the blade with an absorber is uniformly 9 kg/m, and the mass of the absorber is 6 kg (10% blade mass). In the following discussion, the mass of the absorber is kept at the same value. The initial position of the absorber coincides with the pitch axis. When the 1 or 2/rev lagwise load of the two aforementioned blades is compared, the first or second lag frequencies of the two blades are adjusted to be the same by changing the lagwise stiffness. The parameters of the blades are shown in Table 3, and the nondimensional frequencies for the blades are listed in Table 4. Because the lagwise frequencies of the blade change with the variation of the spring stiffness of the absorber, a frequency of $\sqrt{2}\Omega$ for the 1/rev absorber and $\sqrt{5}\Omega$ for the 2/rev absorber are adopted in the table.

In the following investigations, an advance ratio of $\mu = 0.15$ is adopted as the baseline flight state. A wind-tunnel trim method is used to specify steady-state flapping, collective pitch, and cyclic pitches at various flight speeds and thrust levels. The baseline trim values are $C_T = 0.006$, $\beta_{1c} = 0.0$ deg, and $\beta_{1s} = 0.0$ deg. The moment ratio is the ratio of the root bending moment generated by the blade with the absorber to the moment generated by the blade without the absorber.

B. Analysis of the 1/rev Absorber

A 1% critical structural damping is given to the first- and second-order lag modes of the nonrotating blade, and a 5% critical damping

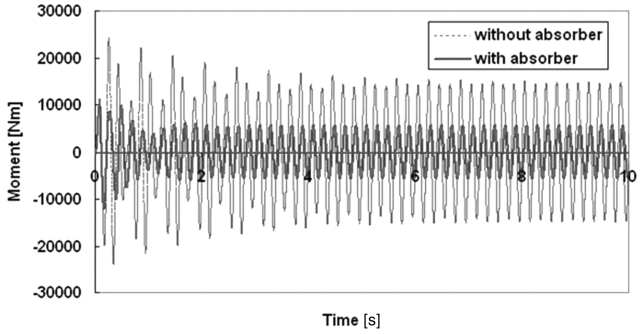

Fig. 14 Lagwise bending moment when $m_a = 6.0$ kg, $f_a = 5.0$ Hz, and $\zeta_a = 0.1$.

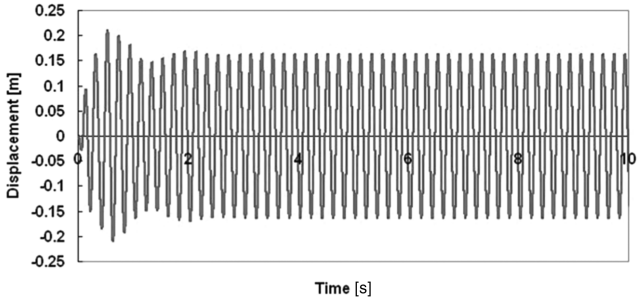

Fig. 15 Absorber displacement when $m_a = 6.0$ kg, $f_a = 5.0$ Hz, and $\zeta_a = 0.1$.

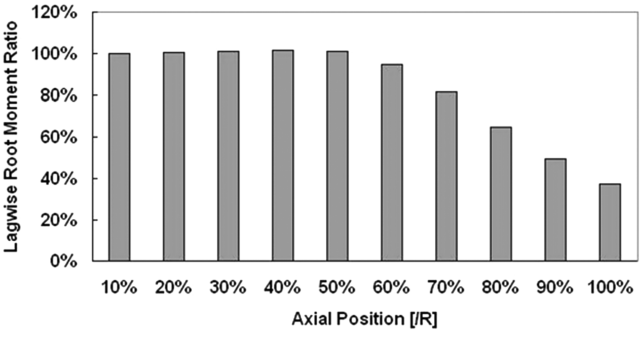

Fig. 16 Influence of absorber position on the lagwise bending moment.

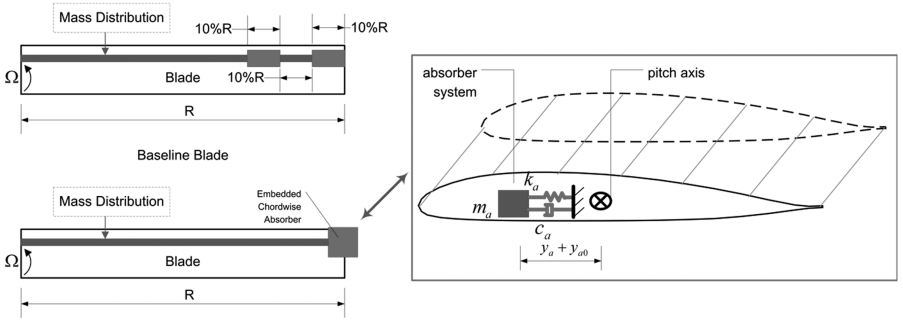

Fig. 17 Configuration of rotor blades with and without absorber.

is provided to the absorber. For different natural frequencies of the absorber, the moment ratios are shown in Fig. 18, which illustrates that the nonrotating tuning frequency of the absorber f_{a0} is about 6.6 Hz.

For vibration reduction, damping could improve the bandwidth and decrease the displacement of the absorber. It also decreases the ability of the absorber. Because of the space restriction of an airfoil cavity, some damping perhaps needs to be provided to the absorber to control the stroke magnitude. The frequency of the absorber is now set to 6.60 Hz. The moment ratios and peak values of the displacement of the absorber with the variation of the damping ratio are shown in Figs. 19 and 20. The steady response of the absorber with 1% critical damping is shown in Fig. 21. These figures illustrate, with the increase in the damping, that the lagwise root bending moment increases and the peak values of the displacement of the absorber decrease. Figure 20 suggests that there is a large static backward movement of the absorber at about 10–15% chord length. In the baseline configuration, the initial location of the absorber is coincident with pitch axis. With the lagwise motion of the blade tip, a centrifugal force component acting on the absorber makes the absorber offset in the chordwise direction, as illustrated in Fig. 22. When chordwise absorbers are designed, the initial chordwise position of the absorber needs to be carefully selected to make the absorber move inside the cavity of the blade. Working with a 1% critical damping, the absorber can absorb about 50% of the 1/rev lagwise root bending moment, which shows that this method is an effective means to reduce the 1/rev lagwise loads for rotor blades.

The frequency of the absorber is kept at 6.60 Hz and the damping ratio at 0.01, and the initial chordwise position is adjusted. The influences of the initial chordwise position of the absorber on the 1/rev lagwise bending moment and the displacement of the absorber are shown in Figs. 23 and 24, respectively. Figure 23 illustrates that moving the absorber forward in the chordwise direction (toward the leading edge) could slightly decrease the lagwise root bending moment. Figure 24 illustrates that the initial position of the absorber could be adjusted to suit the blade cavity. For the consideration of flutter stability, the blade center of gravity is usually designed ahead of pitch axis. It is better to move the absorber ahead of the pitch axis as far as possible.

The influence of the forward speed on the ability of the absorber is shown in Fig. 25, which illustrates that the moments change little with the increase of the forward speed. The influence of the rotor thrust on the ability of the absorber is shown in Fig. 26, which

Table 3 Rotor parameters

Parameter	Value	Parameter	Value
Rotor radius	6 m	Chord length	0.4 m
Number of blades	4	Blade mass	60 kg
Airfoil	NACA 0012	Rotor speed	300 rpm
Pretwist	0 deg		

Table 4 Frequencies of the rotor blade (/rev)

Mode	Baseline	With 1/rev absorber	With 2/rev absorber
First flap	1.13	1.13	1.13
Second flap	3.65	3.59	3.59
Third flap	8.05	8.24	8.24
First lag	1.54	1.54	1.45
Second lag	10.2	9.12	10.2
First torsion	4.70	4.70	4.70

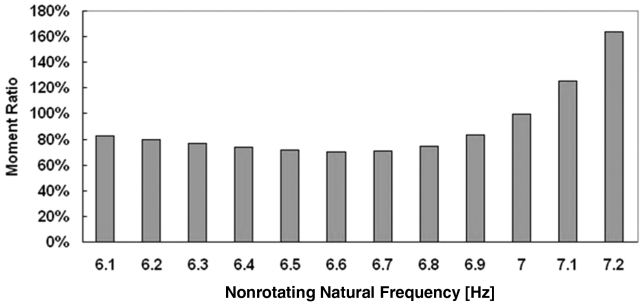

Fig. 18 Influence of tuning frequency on the 1/rev lagwise bending moment.

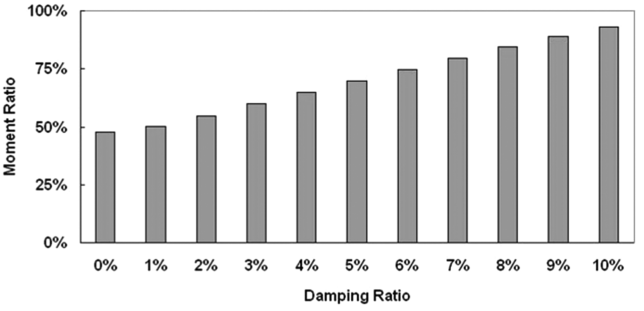

Fig. 19 Influence of the damping on the 1/rev lagwise bending moment (absorber: 6.6 Hz, 6 kg).

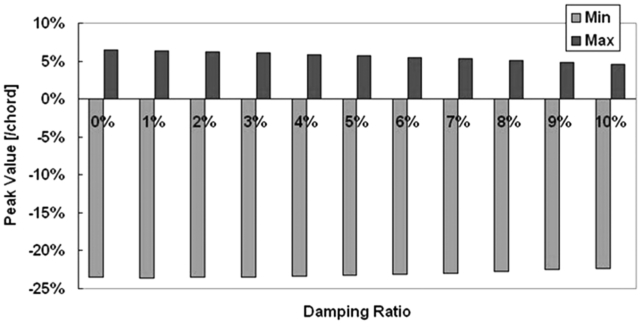

Fig. 20 Influence of the damping on the displacement of the 1/rev absorber (absorber: 6.6 Hz, 6 kg).

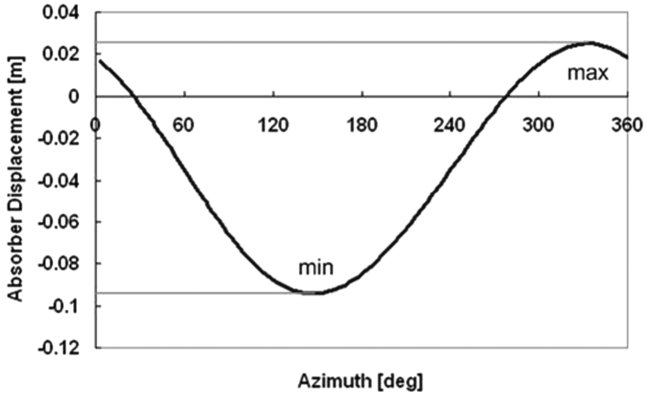

Fig. 21 Steady response of absorber displacement with 1% critical damping.

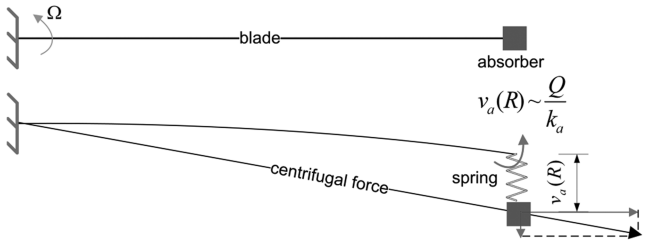

Fig. 22 Absorber offset due to the centrifugal force component.

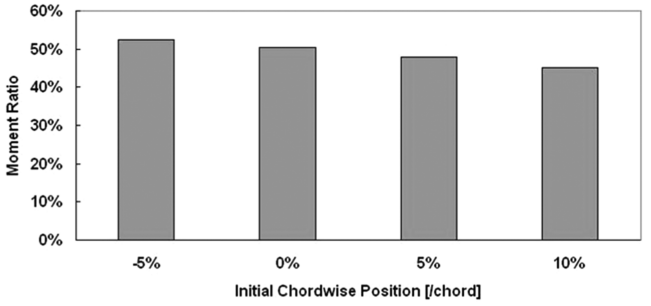

Fig. 23 Influence of absorber chordwise position on the 1/rev lagwise bending moment (absorber: 6.6 Hz, 1% critical damping).

illustrates that the lagwise root bending moment changes little with the increase of the thrust. The influence of rotor trim states on the ability of the absorber is shown in Fig. 27. In this figure, β_{1c} or β_{1s} is kept at zero, when the influence of β_{1c} or β_{1s} is discussed. It can be

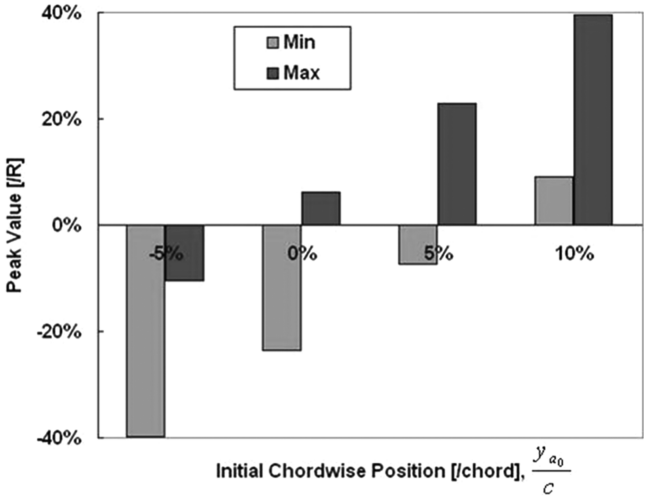

Fig. 24 Influence of absorber chordwise position on the displacement of the 1/rev absorber (absorber: 6.6 Hz, 1% critical damping).

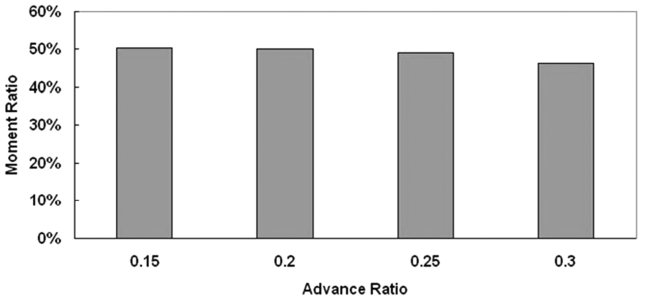

Fig. 25 Influence of forward speed on the ability of the 1/rev absorber (absorber: 6.6 Hz, 1% critical damping).

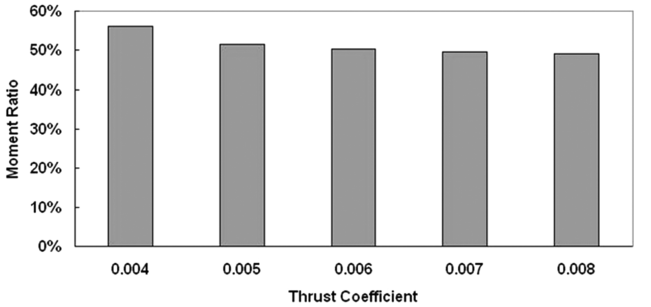

Fig. 26 Influence of thrust on the displacement of the 1/rev absorber (absorber: 6.6 Hz, 1% critical damping).

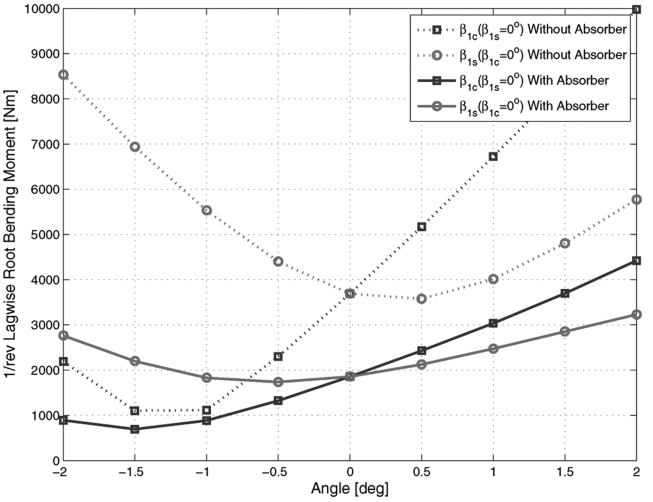

Fig. 27 Influence of trim states on the ability of the 1/rev absorber (absorber: 6.6 Hz, 1% critical damping).

concluded from Fig. 27 that the trim states have a strong influence on the ability of the absorber. In large load states, the absorber works well and could reduce about 50% of the baseline load. The worst design working states of the absorber should be paid attention to, to make sure the absorber can work well under the flight envelop.

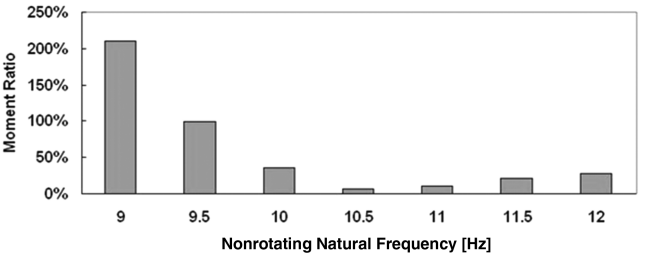

Fig. 28 Influence of tuning frequency on the 2/rev lagwise bending moment (absorber: 5% critical damping).

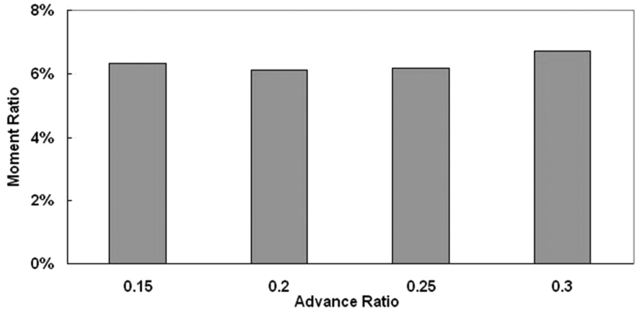

Fig. 29 Influence of forward speed on the ability of the 2/rev absorber (absorber: 10.5 Hz, 5% critical damping).

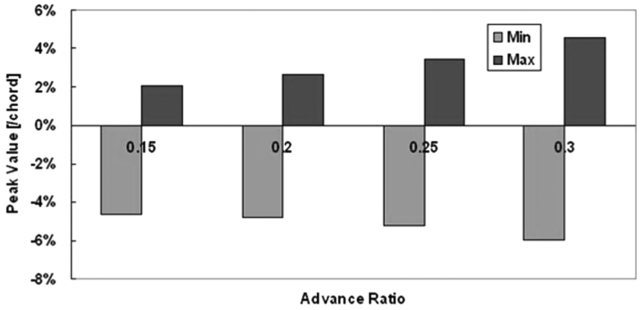

Fig. 30 Influence of forward speed on the displacement of the 1/rev absorber (absorber: 10.5 Hz, 5% critical damping).

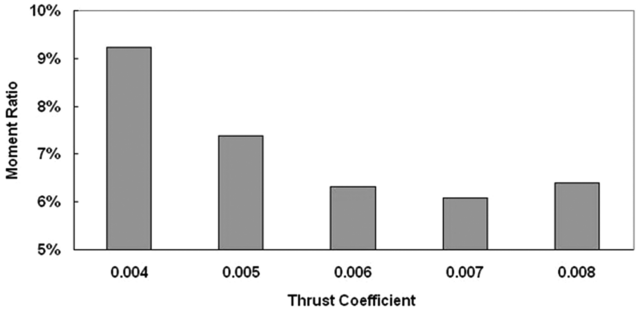

Fig. 31 Influence of rotor thrust on the displacement of the 2/rev absorber (absorber: 10.5 Hz, 5% critical damping).

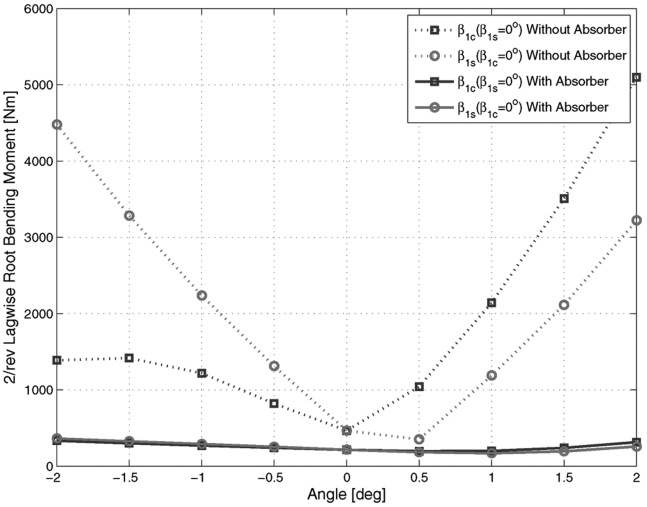

Fig. 32 Influence of trim states on the ability of the 2/rev absorber (absorber: 10 Hz, 1% critical damping).

C. Analysis of the 2/rev Absorber

The major difference between the 1/rev absorber and the 2/rev absorber is the tuning frequency. To reduce the 2/rev lagwise root bending moment, the 2/rev absorber needs to be used. The mass of the 2/rev absorber is 6 kg, and the damping ratio is 5%.

The variation of the moment ratios with respect to the increase in the natural frequency of the absorber is shown in Fig. 28. At the tuning frequency 10.5 Hz, the absorber can absorb about 94% of the 2/rev lagwise root bending moment, which shows that adding a chordwise absorber at the blade tip is more suitable for the higher lagwise loads control. From that figure, the trend is the same as the 1/rev blade-absorber system. In the following cases, the natural frequency of the 2/rev absorber is set to 10.5 Hz.

The influence of the forward speed on the ability of the 2/rev absorber is shown in Fig. 29 and 30. For the 2/rev absorber, the ability to absorb the 2/rev lagwise root bending moment alters little with the increase of forward speed, and the peak values of the displacement of the absorber are reduced significantly compared with the 1/rev absorber. Because the spring stiffness of the 2/rev absorber is much larger than the 1/rev absorber, if absorbing the same value load, the peak values of the displacement of the 2/rev absorber will be reduced significantly.

The influence of rotor thrust on the ability of the absorber is shown in Fig. 31, which illustrates that the lagwise root bending moment changes little with the increase of the thrust.

The influence of rotor trim states on the ability of the 2/rev absorber is shown in Fig. 32. The nonrotating frequency of the absorber is 10.0 Hz, and the damping ratio of the absorber is 1%. That figure illustrates that the trim states have a strong influence on the ability of the absorber. The 2/rev lagwise bending moments with the absorber in small load states do not exceed the large load states. In large load states, the absorber works well and it could reduce about 90% of the baseline load. Compared with Fig. 28, Fig. 32 also illustrates that the optimal tuning frequency of the absorber will vary with respect to the trim states. When designing the tuning absorber, the large load cases need to be paid attention to.

D. Local Large Tip Lagwise Bending Moment

Usually the tips of rotor blades have free boundary conditions. Therefore, the local forces and moments should be zero at the blade tips. However, when the rotor blade tip contains an embedded

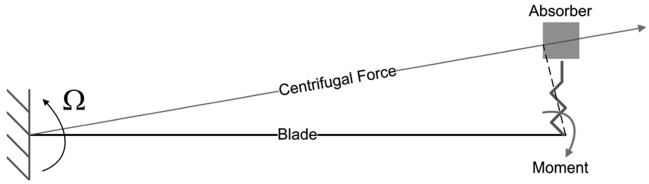

Fig. 33 Configuration of the large tip lagwise bending moment.

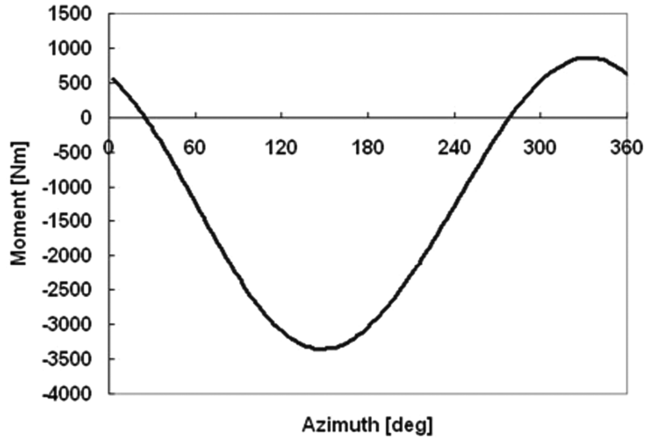

Fig. 34 Steady response of the tip lagwise bending moment (absorber: 6 kg, 6.6 Hz, 1% critical damping).

Appendix: Transformation Matrices Among Different Coordinate Frames

$$[T_{fr}] = \begin{bmatrix} \cos(\beta+\beta_0) & 0 & \sin(\beta+\beta_0) \\ 0 & 1 & 0 \\ -\sin(\beta+\beta_0) & 0 & \cos(\beta+\beta_0) \end{bmatrix} \quad [T_{lf}] = \begin{bmatrix} \cos\zeta & -\sin\zeta & 0 \\ \sin\zeta & \cos\zeta & 0 \\ 0 & 0 & 1 \end{bmatrix} \quad [T_{pl}] = \begin{bmatrix} 1 & 0 & 0 \\ 0 & \cos\theta_p & \sin\theta_p \\ 0 & -\sin\theta_p & \cos\theta_p \end{bmatrix}$$

$$[T_{rs}] = \begin{bmatrix} -\cos\psi & \sin\psi & 0 \\ \sin\psi & \cos\psi & 0 \\ 0 & 0 & -1 \end{bmatrix} \quad [T_{tps}] = \begin{bmatrix} \cos\beta_{1c} & \sin\beta_{1c}\sin\beta_{1s} & \sin\beta_{1c}\cos\beta_{1s} \\ 0 & \cos\beta_{1s} & -\sin\beta_{1s} \\ -\sin\beta_{1c} & \cos\beta_{1c}\sin\beta_{1s} & \cos\beta_{1c}\cos\beta_{1s} \end{bmatrix}$$

$$[T] = \begin{bmatrix} 1-\frac{v'^2}{2}-\frac{w'^2}{2} & v' & w' \\ -(v'\cos\theta_1 + w'\sin\theta_1) & \cos\theta_1(1-\frac{v'^2}{2}) - v'w'\sin\theta_1 & \sin\theta_1(1-\frac{w'^2}{2}) \\ v'\sin\theta_1 - w'\cos\theta_1 & -\sin\theta_1(1-\frac{v'^2}{2}) - v'w'\cos\theta_1 & \cos\theta_1(1-\frac{w'^2}{2}) \end{bmatrix}$$

absorber in the chordwise direction, there is a large lagwise bending moment at the blade tip due to the centrifugal force acting on the absorber, as illustrated in Fig. 33. The response of the tip moment with respect to the azimuth is shown in Fig. 34, in which the rotor response has reached a periodic state. These figures adopt the example in the previous case of the 1/rev absorber analysis with 1% damping. The tip lagwise bending moment can be predicted using $M_{\text{tip}} = m_a \Omega^2 R x_a$. Because this force goes through the rotor shaft, it will generate no moment at the blade root. The large tip moment is proportional to the stroke of the absorber. Reducing the stroke of the absorber is not only for the consideration of the space restriction of the blade cavity, but also for the structural integrity of the blade.

V. Conclusions

In the present paper, an elastomeric absorber is attached to a blade in the chordwise direction to decrease the lagwise loads of stiff in-plane rotor blades. The absorber is modeled as a 1-degree-of-freedom rigid body. The rotor blade is treated as a moderate deflection beam model undergoing coupled flap, lag, and torsion deflections. The equations of motion for the rotor blade with embedded chordwise absorber are derived based on generalized force formulation. Comprehensive parameter influences are conducted to investigate the feasibility of this method to control the rotor lagwise loads. The investigation yielded the following conclusions:

1) For the nonrotating blade, the tuning frequency of the absorber is the excitation frequency. Increasing the mass of the absorber or decreasing the damping of the absorber could help increase the ability of the absorber. The best installation place for the embedded absorber to reduce the lagwise loads is the blade tip.

2) For the rotating blade with the 1/rev embedded elastomeric absorber, decreasing the damping of the absorber could help decrease the lagwise root bending moment. Moving the absorber forward in the chordwise direction, the forward flight and rotor thrust have little influence on the ability of the absorber. The trim states have a strong influence on the ability of the absorber. In large load states, the 1/rev lagwise root bending moment could be reduced to about half of the baseline value.

3) For the rotating blade with the 2/rev embedded elastomeric absorber, forward flight and rotor thrust have little influence on the ability of the absorber. Trim states also have a strong influence on the ability of the absorber. In large load states, the 2/rev lagwise root bending moment could be reduced to about 10% of the baseline value.

4) The major obstacle for the application of the 1/rev elastomeric absorber is the management of the potentially large stroke of the absorber within the restriction of the blade cavity. The large stroke of the absorber may also introduce large local tip lagwise bending moments. These local moments need to be reacted by adequate blade structure.

Acknowledgments

This research was funded by the U.S. Office of Naval Research under grant N00014-06-1-0205 and monitored by John Kinzer and Judah Milgram. The helpful discussions with Kon-Well Wang at Pennsylvania State University are also greatly appreciated.

References

[1] Johnson, W., *Helicopter Theory*, Princeton Univ. Press, Princeton, NJ, 1980, pp. 250–255.

[2] Zapfe, J. A., and Lesieutre, G. A., "Broadband Vibration Damping in Beams Using Distributed Viscoelastic Tuned Mass Absorbers," AIAA Paper 1996-1595, April 1996.

[3] Hébert, C. A., and Lesieutre, G. A., "Rotorcraft Blade Lag Damping Using Highly Distributed Tuned Vibration Absorbers," AIAA Paper 1998-2001, April 1998.

[4] Kang, H., Smith, E. C., and Lesieutre, G. A., "Experimental and Analytical Study of Blade Lag Damping Augmentation Using Chordwise Absorbers," *Journal of Aircraft*, Vol. 43, No. 1, 2006, pp. 194–200. doi:10.2514/1.17074

[5] Kang, H., "Rotor Blade Damping Using Embedded Chordwise Absorbers," Ph.D. Thesis, Pennsylvania State University, University Park, PA, 2001.

[6] Kang, H., Smith, E. C., and Lesieutre, G. A., "The Effects of Embedded Chordwise Absorbers on Blade Aeroelastic Stability," AIAA Paper 2002-1433, April 2002.

[7] Petrie, J. S., Lesieutre, G. A., and Smith, E. C., "Helicopter Blade Lag Damping Using Embedded Fluid Elastic Chordwise Inertial Dampers," AIAA Paper 2004-1950, April 2004.

[8] Petrie, J. S., Lesieutre, G. A., and Smith, E. C., "Design and Model Testing of Helicopter Rotor Blade Lag Fluid Elastic Embedded Chordwise Inertial Dampers," *61st Annual Forum Proceedings of the American Helicopter Society*, American Helicopter Society, Alexandria, VA, June 2005.

[9] Hodges, D. H., and Dowell, E. H., "Nonlinear Equations of Motion for the Elastic Bending and Torsion of Twisted Non-Uniform Blades," NASA TN D-7818, Dec. 1974.

[10] Straub, F. K., Sangha, K. B., and Panda, B., "Advanced Finite Element Modeling of Rotor Blade Aeroelasticity," *Journal of the American Helicopter Society*, Vol. 39, No. 2, 1994, pp. 56–68. doi:10.4050/JAHS.39.56

[11] Zheng, Z. C., Ren, G., and Cheng, Y. M., "Aeroelastic Response of a Coupled Rotor/Fuselage System in Hovering and Forward Flight," *Archive of Applied Mechanics*, Vol. 69, No. 1, 1999, pp. 68–82. doi:10.1007/s004190050205

[12] Keller, J. A., "Analysis and Control of the Transient Aeroelastic Response of Rotors During Shipboard Engagement and Disengagement Operations," Ph.D. Thesis, Pennsylvania State University, University Park, PA, 2001.

[13] Peters, D. A., and HaQuang, N., "Dynamic Inflow for Practical Application," *Journal of the American Helicopter Society*, Vol. 33, No. 4, 1988, pp. 64–68. doi:10.4050/JAHS.33.64

[14] Owen, D. R. J., and Hinton, E., *Finite Elements in Plasticity: Theory and Practice*, Pineridge Press, Swansea, Wales, UK, 1980, pp. 431–436.
[15] Bagai, A., "Contribution to the Mathematical Modeling of Rotor Flow-Fields using a Pseudo-Implicit Free-Wake Analysis," Ph.D. Thesis, University of Maryland, College Park, MD, 1995.
[16] Leishman, J. G., *Principles of Helicopter Aerodynamics*, 1st ed., Cambridge Univ. Press, Cambridge, England, UK, 2000, pp. 142–153.
[17] Grover, G. K., *Mechanical Vibration*, 6th ed., Roorker Press, Roorkee, India, 1998, pp. 228–243.